Octacalcium Phosphate Carboxylates. 2. Characterization and Structural Considerations

Milenko Marković,*[1a,c] Bruce O. Fowler,[1b] and Walter E. Brown[1a,d]

American Dental Association Health Foundation, Paffenbarger Research Center, National Institute of Standards and Technology, Gaithersburg, Maryland 20899, and National Institute of Dental Research, NIH, Bone Research Branch Research Program, National Institute of Standards and Technology, Gaithersburg, Maryland 20899

Received March 18, 1993. Revised Manuscript Received July 30, 1993®

Detailed physicochemical characterization of octacalcium phosphate carboxylates (OCPCs) with structurally incorporated succinate, adipate, suberate, sebacate, fumarate, and citrate ions is reported. Compositional formulas of the OCPCs were derived from Ca, P, C, H, and H_2O analyses. In octacalcium phosphate dicarboxylates with the general formula $Ca_8(HPO_4)_{2-x}$(dicarboxylate)$_x(PO_4)_4 \cdot yH_2O$, a maximum of one HPO_4^{2-} was replaced by a dicarboxylate ion ($x \leq 1$). The water content increased with increasing chain length of the dicarboxylate ion ($5.7 \leq y \leq 8.0$). For octacalcium phosphate tricarboxylate, $Ca_8(HPO_4)_{2-1.5x}$(tricarboxylate)$_x(PO_4)_4 \cdot yH_2O$, with incorporated citrate ions the values of x and y were 0.4 and 7.8, respectively. X-ray diffraction patterns of OCPCs show structural similarity with the parent compound octacalcium phosphate (OCP); the b and c axes of the unit cells were nearly the same as those of OCP but the a axes were progressively expanded concomitant with carbon chain length. Infrared and Raman assignments were made for nearly all bands of these six OCPCs; an OCP-succinate containing the deuterated succinate ion was prepared to facilitate band assignments. Spectra of the OCPCs, as compared to that of OCP, showed the presence of carboxylate groups, changes in water bonding, only slight changes in PO_4 environments, and preferential reduction in $HPO_4(5)$ content. OCP has two crystallographically nonequivalent HPO_4 groups (designated 5 and 6); the preferential replacement of $HPO_4(5)$ by the dicarboxylate ion is plausible considering lattice geometry. By utilizing combined data from the different methods, the possible positions of carboxylate ions in the OCPC structures are discussed.

Introduction

The family of new compounds named octacalcium phosphate carboxylates (OCPCs) with general formula $Ca_8(HPO_4)_m$(carboxylate)$_n(PO_4)_4 \cdot yH_2O$ has structural similarities[2-5] with the parent compound[6-8] octacalcium phosphate (OCP), $Ca_8(HPO_4)_2(PO_4)_4 \cdot 5H_2O$. The presence of di- or tricarboxylate ions in the OCPC structure caused an a-axis lattice expansion[3,5] compared to that of pure OCP. An expansion of about 40% occurred when the long-chain dicarboxylate with 8 (suberate) or 10 (sebacate) carbon atoms was incorporated[5] and this appears to be the upper limit to maintain the OCP-like structure.

Preparative conditions and identification of a series of OCPCs with incorporated saturated and unsaturated dicarboxylates, and tricarboxylate, were described in part 1[5] of this work. Here in part 2, detailed chemical and physical characterization of OCP-succinate (OCP-SUCC), OCP-adipate (OCP-ADIP), OCP-suberate (OCP-SUB), OCP-sebacate (OCP-SEB), OCP-fumarate (OCP-FUM), and OCP-citrate (OCP-CIT) is reported. Compositional formulas were determined and structural details were elucidated by comparing vibrational spectra and X-ray diffraction patterns of the OCPCs with those of OCP. Some of these compounds may be formed as precursors or intermediates in mitochondria and in biomineralization processes.[5]

Experimental Section[22]

Materials. The OCPCs and OCP were synthesized as described in part 1[5] and part 3,[9] respectively. A deuterated succinate analogue of OCP-succinate was prepared according to the general method[5] utilizing $(CD_2)_2(COOH)_2$ (98 atom % D, Aldrich) with initial and final pH of suspensions 6.24 and 6.78, respectively, and a reaction time of 24 h.

Analytical Techniques. Calcium was determined by atomic absorption spectroscopy with a Perkin-Elmer Model 603 spectrophotometer using an air–acetylene flame and the 422.7-nm wavelength line. Analyses were performed directly on 250 ± 0.12 mL solutions that all contained 1000 ppm $LaCl_3$ and weighed amounts (precision ±0.1%) of standards (calcium carbonate, NIST standard reference material, dried at 250 °C for 2 h) and samples to give an absorbance of about 0.400 (instrumental uncertainty of 0.001 absorbance unit). The calcium concentrations of unknown solutions were determined using two or more weighed bracketing standards that were within ±2% relative to the unknown values. The precision of replicate measurements determined as coefficient of variation (CV) was ±0.4%. Phos-

* Abstract published in *Advance ACS Abstracts*, September 15, 1993.

(1) (a) American Dental Association Health Foundation, PRC. (b) National Institute of Dental Research, NIH. (c) On leave of absence from the Rudjer Bošković Institute and the Faculty of Science, University of Zagreb, Zagreb, Croatia. (d) Deceased.

(2) Monma, H.; Goto, M. *Bull. Chem. Soc. Jpn.* **1983**, *56*, 3843.

(3) Monma, H. *Bull. Chem. Soc. Jpn.* **1984**, *57*, 599.

(4) Marković, M.; Fowler, B. O.; Brown, W. E. *J. Dent. Res.* **1988**, *67*, 270 (Abstract 1259).

(5) Marković, M.; Fowler, B. O.; Brown, W. E. *Chem. Mater.*, first of three papers in this issue.

(6) Brown, W. E.; Lehr, J. R.; Smith, J. P.; Frazier, A. W. *J. Am. Chem. Soc.* **1957**, *79*, 5318.

(7) Brown, W. E. *Nature* **1962**, *196*, 1048.

(8) Mathew, M.; Brown. W. E.; Schroeder, L. W.; Dickens, B. *J. Crystallogr. Spectrosc. Res.* **1988**, *18*(3), 235.

(9) Fowler, B. O.; Marković, M.; Brown, W. E. *Chem. Mater.*, third of three articles in this issue.

0897-4756/93/2805-1406$04.00/0

Table I. Chemical and Thermogravimetric Analyses[a] of Octacalcium Phosphate Carboxylates (OCPC)

		chemical analyses				water content		TGA		
OCPC	sample no[b]	Ca	P	C	H	H_2O[c]	H_2O[d]	total loss	H_2O[e]	temp (°C)
OCP-SUCC	11	31.44	15.44	4.44	1.46	10.4	9.0			
	12	31.22	15.24	4.62	1.61	10.8	10.2	10.9	10.2	520
	13	31.47	15.57	4.19	1.56	10.5	10.1			
	14	31.42	15.31	4.25	1.57	11.2	10.1	11.6	10.9	500
	15	31.14	15.36	4.79	1.60	10.1	10.0	10.8	10.1	490
	16	31.51	15.57	4.08	1.50	10.8	9.7	11.5	10.8	540
OCP-ADIP	21	30.84	15.49	5.59	1.75	10.4	9.3	11.0	10.3	480
	24	30.68	15.07	6.10	1.86	10.9	9.8	11.8	10.1	460
OCP-SUB	25	29.64	14.83	6.78	2.18	12.6	11.2	12.0	11.3	460
	26	28.61	14.32	7.46	2.22	14.0	10.7	12.3	11.7	500
OCP-SEB[f]	31	31.94	16.29	5.72	1.89					
	33	32.66	16.80	4.33	1.39					
OCP-FUM	37	31.40	15.74	3.87	1.16	11.1	8.1	10.5	9.8	600
	38	32.30	16.24	3.60	1.14	9.3	8.0	10.6	9.8	600
OCP-CIT	46	30.72	15.37	2.69	1.50	15.0	11.0	12.9	12.2	450
	48	31.26	15.90	2.91	1.38	12.3	9.7	12.6	11.9	470

[a] All values in mass %. [b] These correspond to sample numbers in part 1.[5] [c] Calculated from total mass less sum of analyzed constituents. [d] Calculated from hydrogen content. [e] Calculated from total mass loss less water from pyrolyzed hydrogen phosphate. [f] Water data not included because these samples contain several other compounds.

phate was determined as the phosphovanadomolybdate complex[10] using a Cary Model 219 spectrometer and a wavelength of 420 nm. The phosphate solutions (100 ± 0.08 mL) contained weighed amounts (±0.1%) of standards (KH_2PO_4, Baker Ultrex Reagent, dried at 105 °C for 2 h) and unknowns to give an absorbance of about 0.800 (instrumental uncertainty of 0.001 absorbance unit). Absorbances were obtained at essentially the same age time of color development (~30 min) in the same sample cell versus a H_2O blank (differential absorbance measurement[10] was not used). Precision of replicate determinations (CV) was ±0.2% relative.

Carbon, hydrogen, and nitrogen were determined by chemical microanalysis (Galbraith Laboratories, Knoxville, TN). The content of nitrogen was less than 0.2 mass % (detection limit). Precisions of carbon and hydrogen analyses were ±4.6% and ±7.1%, respectively.

Thermogravimetric analysis (TGA) was performed using a Perkin-Elmer Model TGS-2, scan rate 20 °C/min, in the temperature range 37–800 °C in a nitrogen atmosphere.

Scanning electron micrographs, obtained from dried OCPCs crystals using a JEOL Model JSM-5300, showed platelike crystal morphology with length dimensions from 3 to 10 μm, except for OCP-CIT crystals with length <1 μm.

X-ray Diffraction. X-ray diffraction (XRD) patterns of the powdered samples (particle size <5 μm) were obtained in the 3–66° 2θ range with Cu Kα radiation using a Rigaku X-ray diffractometer operating at 40 kV and 25 mA. Interplanar spacings (*d* values) were obtained from averages of triplicate degree 2θ recordings expanded to have a measurement precision of ±0.006°.

Infrared Spectroscopy. Infrared spectra (IR) from 4000 to 300 cm^{-1} were recorded using a Perkin-Elmer Model 621 spectrophotometer purged with dry CO_2-free air. The "split" oil mull technique, fluorolube from 4000 to 1310 cm^{-1} and Nujol from 1320 to 300 cm^{-1}, was used to obtain spectra. The OCPC samples were gently hand-mulled in the respective oils to a particle size of less than 5 μm, and the slurries were contained between Tl(Br,I) plates. To normalize bands for intensity comparisons that occur in the separate fluorolube and Nujol spectral regions, sample concentrations of all the OCPCs were first adjusted for the Nujol range to give about the same intensity of the PO_4 bands in the 600–500-cm^{-1} range; then concentrations for the fluorolube range were adjusted to equal the intensities (within ±5%) of the OCPC bands in the Nujol range at about 1560 or 1630 cm^{-1} that were unobscured by CH_x bands. The KBr pressed pellet technique was not used because the minimum pressure, about 275 MPa, required to form transparent pellets suitable for spectral recordings caused structural changes in these OCPCs as evidenced by differences in their spectra obtained from pressed KBr pellets and oil mulls. A spectroscopic account of the pressure induced changes in these OCPCs will be given elsewhere.[11] The wavenumber accuracy, calibrated against standard indene bands,[12] was ±2 cm^{-1}. Spectral slit widths were about 6 cm^{-1} above 2000 cm^{-1} and 3–5 cm^{-1} below 2000 cm^{-1}.

Raman Spectroscopy. Raman spectra were obtained using the procedure and instrumentation described in part 3.[9] Spectra in Figure 5 were recorded from pressed pellets (pressing conditions given in part 3[9]) using 175–200 mW of 488.0-nm excitation and a spectral slit width of 5 cm^{-1}. To normalize bands of OCP and the OCPCs for intensity comparison, the intensities of PO_4 bands at about 426 cm^{-1} were instrumentally adjusted to have nearly the same intensities (within ±5%). Sample pellets were aged in the laser beam for about 1–4 h to reduce sample fluorescence before recordings. Spectra were also recorded using 514.5-nm excitation to discern, in most cases, sample bands from spurious ghost bands. The wavenumber accuracy was ±2 cm^{-1}.

Results

Chemical Characterization. In Table I, chemical analyses (Ca, P, C, H) for six OCPCs are given. Water content data were determined by three independent procedures; from mass balance, from hydrogen content data, and from TG curves. The values of mass % H_2O calculated from hydrogen content data (Table I) were systematically lower but, by taking into account the small amount of hydrogen in analyzed samples (1–2%) which derived from both polycarboxylate and water, and uncertainty in hydrogen determinations, the agreement with other methods was satisfactory. Total mass loss determined by TGA (Table I) corresponds to the content of zeolitic and coordination water and to the water content from pyrolyzed hydrogen phosphate.[13] In Figure 1, TG curves for OCP-SUB, OCP-FUM, and OCP-CIT are shown. The shape of the curve for OCP-SUB corresponds to those of OCP-SUCC and OCP-ADIP. For OCP-SUB, the major amount of water (~90%) was lost in the temperature range 37–180 °C, and an additional ~10% at 180–500 °C which includes water from pyrolyzed hydrogen phosphate. For OCP-CIT, ~70% of the water was lost below 180 °C and the remainder between 180 and 460 °C, while OCP-FUM lost ~60% below 180 °C and ~40% between 180 and 600 °C. The corrected calculated

(10) Gee, A.; Deitz, V. R. *Anal. Chem.* **1953**, *25*, 1320.

(11) Fowler, B. O.; Marković, M. Manuscript in preparation.

(12) Jones, R. N.; Nadeau, A. *Spectrochim. Acta* **1964**, *20*, 1175.

(13) Fowler, B. O.; Moreno, E. C.; Brown, W. E. *Arch. Oral Biol.* **1966**, *11*, 477.

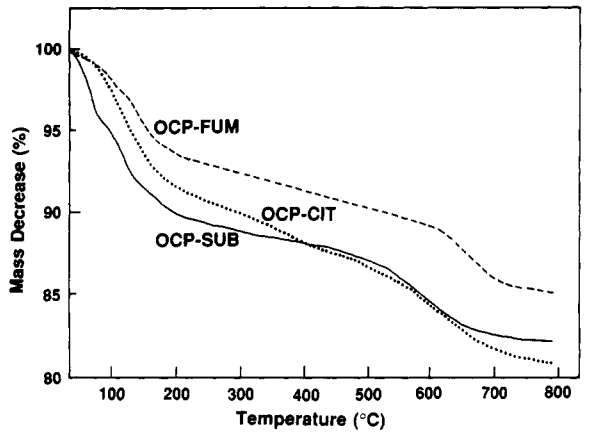

Figure 1. TG curves for OCP-CIT, OCP-FUM, and OCP-SUB.

mass % of H_2O from TGA showed very good agreement with the values determined from mass balance (Table I).

Compositions of the OCPCs, calculated from chemical analyses in Table I, are given in Table II. By normalizing the composition on the basis of eight calcium ions, the total number of phosphate ions (PO_4^{3-} and HPO_4^{2-}) was obtained from the Ca/P molar ratio. The number of carboxylate ions (x) was determined from the carbon analysis data. The content of HPO_4^{2-} was calculated using the general formulas[3] for OCP-dicarboxylates and OCP-tricarboxylates, $Ca_8(HPO_4)_{2-x}(\text{dicarboxylate})_x(PO_4)_4 \cdot yH_2O$ and $Ca_8(HPO_4)_{2-1.5x}(\text{tricarboxylate})_x(PO_4)_4 \cdot yH_2O$, respectively: (I) from the number of carboxylate ions, and (II) from total number of phosphate ions in excess of four PO_4^{3-}. The agreement between HPO_4^{2-} values (I and II) for the OCP dicarboxylates verified the general formula. For OCP-SEB the HPO_4^{2-} values are in disagreement because these samples contained several other compounds (nonstoichiometric hydroxyapatite ("HA"), OCP, calcium sebacate monohydrate). The number of HPO_4^{2-} in OCP-CIT determined on the basis of citrate content is 0.17 ± 0.06 units higher than the number of HPO_4^{2-} determined in excess of four PO_4^{3-} (Table II).

From the average number of dicarboxylate ions for each salt (Table II), the compositional (empirical) formulas were established. The estimate of the standard deviations of the number of HPO_4^{2-} and carboxylate ions per corresponding average formula of OCP-dicarboxylate is ±0.07. The number of water molecules per unit formula was determined using the water content calculated from mass balance. The estimate of the standard deviation of the number of H_2O per corresponding average formula of OCP-dicarboxylate is ±0.4. The compositional formula of OCP-CIT showed larger deviations in the number of HPO_4^{2-} and H_2O molecules.

XRD. The XRD powder patterns of OCP, OCP-CIT, OCP-FUM, OCP-SUCC, and OCP-SUB are shown in Figure 2. Generally, the patterns are ordered from top to bottom with decreasing 2θ value for the (100) diffraction line. The designated (100), (010), and (002) diffraction lines in the XRD pattern of OCP correspond to a, b, and c axis of its unit cell, respectively. In the left part of Figure 2, the strong (100) diffraction lines are shown expanded and on scale. The decimal number by each line denotes the ratio between intensities of the (100) diffraction line shown in the left and in the right parts of Figure 2. This is useful for comparing the (100) intensities with other lines in the XRD pattern. The d_{100}, d_{010}, and d_{002} values for OCP and all OCPCs are listed in Table III.

Infrared Spectra. IR transmittance spectra of OCP, OCP-CIT, OCP-FUM, OCP-SUCC, and OCP-SUB are shown in the 4000–300-cm^{-1} range in Figure 3 and with an expanded abscissa scale from 1750 to 300 cm^{-1} in Figure 4. Some of the weak OCP and OCPC bands in the 800–700-cm^{-1} region (not listed in Table IV) arise from the baseline (BL). The band wavenumbers and assignments are given in Table IV. The OCP and OCPC band assignments for PO_4, HPO_4, and H_2O modes are from part 3;[9] previous assignments for COO modes,[14,15] CH_2 modes,[16a,17] and CH modes[16b] were utilized to identify and assign bands of these modes in OCPC spectra.

Raman Spectra. Raman spectra of OCP, OCP-CIT, OCP-FUM, OCP-SUCC, and OCP-SUB are shown in the 4000 to 200-cm^{-1} range in Figure 5. The numerous sharp bands in the baseline (BL) arise from grating ghosts and their presence in spectra are denoted under braces and by short vertical lines. In the OCP spectrum, the broad ascending Raman intensity from about 1500 to 4000 cm^{-1} originated from fluorescence from the irradiated OCP; the OCPC samples, overall, showed less fluorescence. The OCP-SUB spectrum (denoted by a), recorded at lower intensity expansion, has its very strong ν_1 PO_4 band at 960 cm^{-1} on scale for relative band intensity comparisons; the OCP-SUB insert (denoted by b) is an abscissa scale expansion of the ν_1 PO_4 band that reveals the second band at 966 cm^{-1} on the major band at 960 cm^{-1}. The ν_1 PO_4 bands of all other spectra are off scale, and all, except OCP-CIT, have a shoulder or band at about 964–966 cm^{-1} on the major band at 957–960 cm^{-1}. The band wavenumbers and assignments are given in Table V. The OCP and OCPC band assignments for PO_4, HPO_4, and H_2O modes are from part 3;[9] previous assignments for COO modes,[15,18a] CH_2 modes,[17,18b] and CH modes[18c] were utilized to identify and assign bands of these modes in OCPC spectra.

The IR and Raman band wavenumbers and assignments for OCP-SUCC and its deuterated analogue, OCP-C_2D_4-$(COO)_2$, in the 1600–1300-cm^{-1} range are given in Table VI.

Discussion

Compositional Formulas. Compositional formulas of the OCPCs derived from the formula of OCP show a reduction in the number of HPO_4^{2-} caused by the incorporation of di- and tricarboxylate ions in the structure. In the OCPCs a maximum of one HPO_4^{2-} per unit formula (two per unit cell) can be replaced by a dicarboxylate ion, $0.8 \leq x \leq 1.0$ (Table II). This finding suggests that only one of the two different positions of HPO_4^{2-} ions in the OCP structure[8] is capable of exchange without drastic structural changes. The content of water in the OCP-dicarboxylates increases with increasing chain length of the dicarboxylate ions, $5.7 \leq y \leq 8.0$ (Table II).

For OCP-CIT there is disagreement between HPO_4^{2-} values calculated from the Ca/P ratio and from the content

(14) Nakamoto, K. *Infrared Spectra of Inorganic and Coordination Compounds*; John Wiley & Sons, Inc.: New York, 1963; p 197.
(15) Marcos, J. I.; Marquez, F.; Arenas, J. F. *Anal. Quim.* **1978**, *74*, 1345.
(16) (a) Alpert, N. L.; Keiser, W. E.; Szymanski, H. A. *IR Theory and Practice of Infrared Spectroscopy*; Plenum Press: New York, 1964; p 193; (b) p 249.
(17) Suzuki, M.; Shimanouchi, T. *J. Mol. Spectrosc.* **1968**, *28*, 394.
(18) (a) Dollish, F. R.; Fateley, W. G.; Bentley, F. F. *Characteristic Raman Frequencies of Organic Compounds*; John Wiley & Sons: New York, 1974; p 110; (b) Chapter 1; (c) Chapter 6.

Table II. Composition of Octacalcium Phosphate Carboxylates Calculated from Chemical Analyses and General Formulas: $Ca_8(HPO_4)_{2-x}$(dicarboxylate)$_x(PO_4)_4 \cdot yH_2O$ for Dicarboxylates and $Ca_8(HPO_4)_{2-1.5x}$(tricarboxylate)$_x(PO_4)_4 \cdot yH_2O$ for Tricarboxylates

OCPC	sample no[a]	Ca/P molar ratio	$PO_4 + HPO_4$	polycarb x	HPO_4 I[b]	HPO_4 II[c]	H_2O[d] y	compositional formula[e]
OCP-SUCC	11	1.574	5.08	0.94	1.06	1.08	5.9	
	12	1.583	5.05	0.99	1.01	1.05	6.2	
	13	1.562	5.12	0.89	1.11	1.12	5.9	$Ca_8(HPO_4)_{1.07}(succ)_{0.93}(PO_4)_4 \cdot 6.0H_2O$
	14	1.586	5.04	0.90	1.10	1.04	6.3	
	15	1.567	5.10	1.03	0.97	1.10	5.8	
	16	1.564	5.11	0.86	1.14	1.11	6.1	
OCP-ADIP	21	1.538	5.20	0.79	1.21	1.20	6.0	$Ca_8(HPO_4)_{1.17}(adip)_{0.83}(PO_4)_4 \cdot 6.2H_2O$
	24	1.573	5.09	0.88	1.12	1.09	6.3	
OCP-SUB	25	1.545	5.18	0.76	1.24	1.18	7.6	$Ca_8(HPO_4)_{1.18}(sub)_{0.82}(PO_4)_4 \cdot 8.0H_2O$
	26	1.544	5.18	0.87	1.13	1.18	8.4	
OCP-SEB[f]	31	1.515	5.28	0.48	1.52	1.28		
	33	1.502	5.33	0.35	1.65	1.33		
OCP-FUM	37	1.542	5.19	0.82	1.18	1.19	6.3	$Ca_8(HPO_4)_{1.22}(fum)_{0.78}(PO_4)_4 \cdot 5.7H_2O$
	38	1.537	5.20	0.74	1.26	1.20	5.1	
OCP-CIT	46	1.544	5.18	0.39	1.41	1.18	8.7	$Ca_8(HPO_4)_{1.40}(cit)_{0.40}(PO_4)_4 \cdot 7.8H_2O$
	48	1.519	5.27	0.41	1.38	1.27	7.0	

[a] Same designation as in Table I. [b] Calculated from polycarboxylate content. [c] Calculated from total phosphate content. [d] Calculated from water content, H_2O,[c] in Table I. [e] From average values. [f] Formula not calculated because these samples contain several other compounds.

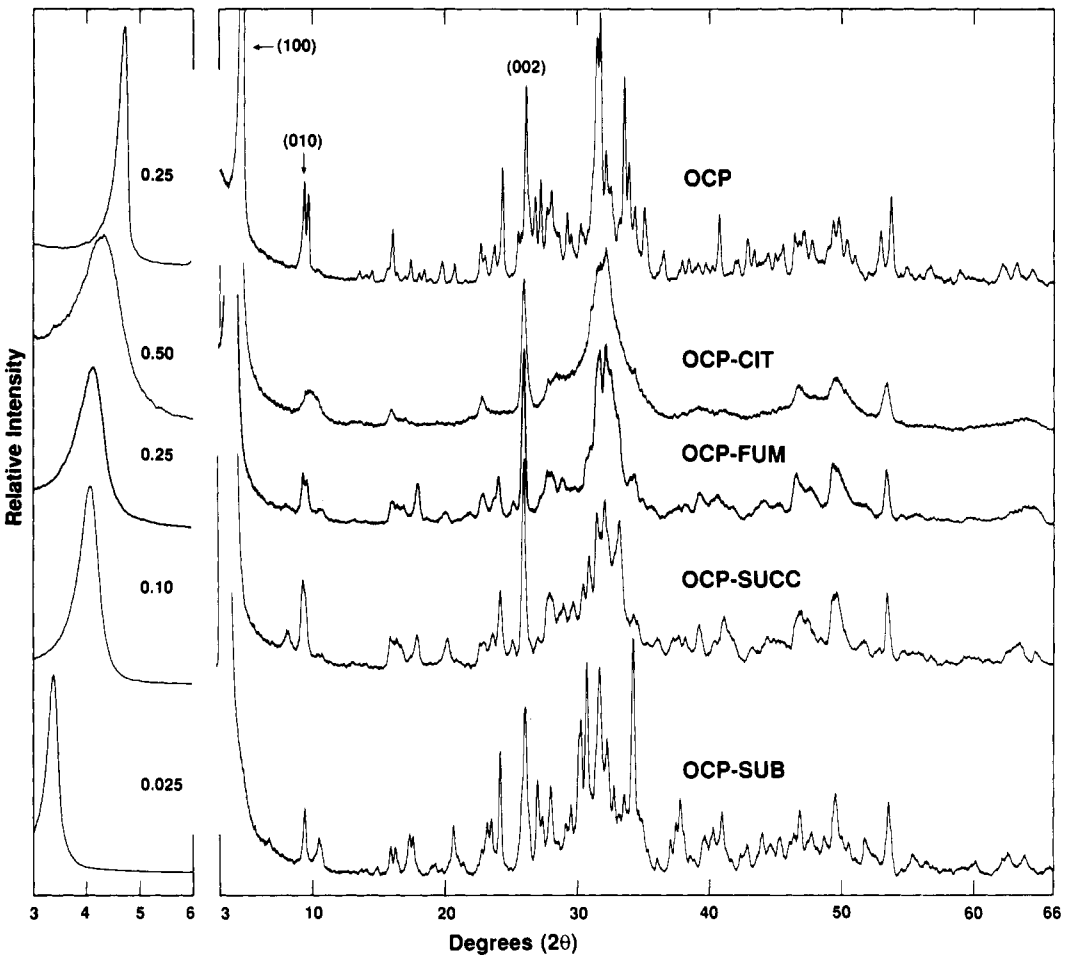

Figure 2. XRD patterns for OCP, OCP-CIT, OCP-FUM, OCP-SUCC, and OCP-SUB. In the left part the expanded scale for 2θ between 3 and 6° is given. The decimal numbers denote the ratio between intensities of the (100) diffraction line shown in the left and in the corresponding right parts.

of citrate^{3-} ions (Table II). The possibility that this disagreement is caused by a citrate ion charge less than −3 (COOH group(s) in the structure) was ruled out by spectral data; COOH bands were not detected, only COO bands were found (Tables IV and V). Calculation on the basis of charge balance shows an excess of PO_4^{3-} ions compared to the general formula, indicating additional apatitic layers in the OCP-CIT or simply a physical mixture of OCP-CIT and HA. The best estimate is the presence of ~83% of $Ca_8(HPO_4)_{1.30}(cit)_{0.47}(PO_4)_4 \cdot 8H_2O$ and ~17% of HA. Consistent with this, a weak HA band at 3570 cm^{-1} (OH stretch) was present in Raman spectra of OCP-CIT.

XRD. The OCPC patterns are similar to that of OCP. The broadened diffraction lines for OCP-FUM and especially OCP-CIT indicate less crystalline materials com-

Table III. Observed *d* Values (nm) for Octacalcium Phosphate Carboxylates (OCPC) Corresponding to *a*-, *b*-, and *c*-Axis Dimensions

OCPC	d_{100}	d_{010}	d_{002}
OCP	1.868(2)	0.938(1)	0.3414(2)
OCP-SUCC	2.13(1)	0.943(1)	0.3420(2)
OCP-ADIP	2.37(1)	0.938(1)	0.3425(2)
OCP-SUB	2.62(1)	0.942(1)	0.3419(2)
OCP-SEB	2.59(2)	0.945(2)	0.3431(2)
OCP-FUM	2.15(1)	0.942(1)	0.3421(2)
OCP-CIT	2.05(2)	0.897(2)	0.3429(2)

pared to the well-crystallized OCP standard and OCPCs containing saturated dicarboxylates (Figure 2). This line broadening can be explained by possible structural imperfection and in addition by small size (<1 μm) of the OCP-CIT crystals. The higher crystallinity of the OCPCs containing saturated dicarboxylate ions having higher symmetry plausibly arises from more ordered repeating structural units. Moreover, they have unusually high (100) intensities; the OCP-SUB (100) line intensity is about 10 times that of OCP, and its pattern has several other high intensity lines in the region of $20 < 2\theta < 40°$ that may arise from multiples of the (100) line.

The d_{100} values for OCPCs are larger than that of OCP (Table III); this expansion generally correlates with increasing length of the carbon chain (see part 1[5] for details). The d_{010} values for OCP and all OCPCs except OCP-CIT are almost identical; the OCP-CIT d_{010} value is significantly lower compared to OCP (~5%). The d_{002} values, within experimental error, are the same for all compounds. These data show that the unit-cell parameters of the OCPCs, except the *a* axis which is expanded, are not significantly changed from those of OCP.

Infrared Spectra. *(1) PO_4 and HPO_4 Bands. OCP-SUCC, OCP-ADIP, OCP-SUB, and OCP-FUM*: The ν_3, ν_1, ν_4, and ν_2 PO_4 band positions and intensities of these OCPCs are very similar to those of OCP; this indicates the apatite-like structural domains in these OCPCs are very similar to that in OCP. The ν_1 PO_4 band shows a shoulder at about 970 cm^{-1}, a probable second ν_1 component, and the ν_3 PO_4 component at about 1026 cm^{-1} (about 3 cm^{-1} lower in OCP) indicate slight changes in PO_4 groups.

In these OCPCs the bands attributed to $HPO_4(6)$ in OCP at 1295 and 917 cm^{-1} are still present at about the same wavenumbers and intensities except for OCP-FUM which has broadened and lower intensity bands. This indicates $HPO_4(6)$ is still present in OCP-SUCC, OCP-ADIP, and OCP-SUB with minor change. The bands assigned to $HPO_4(5)$ at 1193 and 861 cm^{-1} in OCP are missing except for a weak band at about 864 cm^{-1} in OCP-FUM. These changes indicate the $HPO_4(5)$ group is missing or substantially reduced in these OCPCs. The OCP band at 524 cm^{-1} assigned to both $HPO_4(5$ and $6)$ has considerably reduced intensity in all four OCPCs which further attests to their reduced HPO_4 contents. In OCP-SUCC, OCP-ADIP, and OCP-SUB, the ν_3 HPO_4 component at about 1124 cm^{-1} retains strong intensity while the ν_3 HPO_4 component at 1107 cm^{-1} is considerably reduced in intensity. Since changes in other bands show $HPO_4(6)$ is still present and $HPO_4(5)$ is considerably reduced, the bands at 1124 and 1107 cm^{-1} are assigned to $HPO_4(6)$ and $HPO_4(5)$, respectively. These data were used to assign these bands to the different HPO_4 groups in OCP in part 3.[9]

OCP-SEB. The OCP-SEB spectrum showed bands corresponding to both $HPO_4(5$ and $6)$ groups due to the presence of an additional phase of OCP (also detected by XRD); this precluded discerning preferential changes in these ions except for an overall reduction in HPO_4 content.

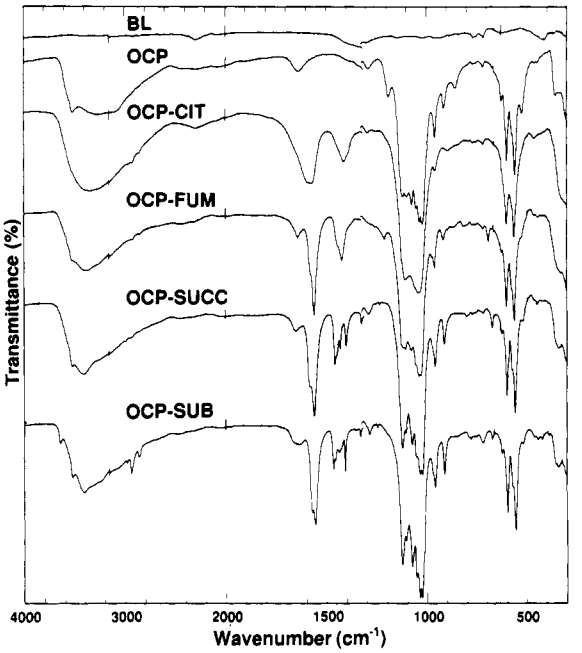

Figure 3. Infrared transmittance spectra of OCP, OCP-CIT, OCP-FUM, OCP-SUCC, and OCP-SUB recorded from fluorolube mulls, 4000 to 1310 cm^{-1}, and Nujol mulls, 1320–300 cm^{-1}. BL denotes the oil mull baseline.

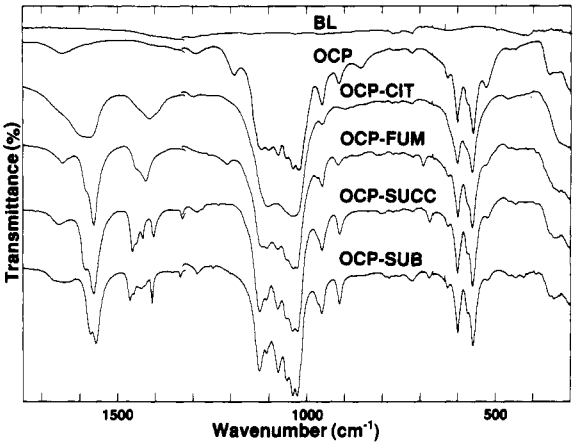

Figure 4. Infrared transmittance spectra of OCP, OCP-CIT, OCP-FUM, OCP-SUCC, and OCP-SUB recorded from fluorolube mulls, 1750–1310 cm^{-1}, and Nujol mulls, 1320–300 cm^{-1}. BL denotes the oil mull baseline.

OCP-CIT. The OCP-CIT spectrum is poorly resolved and mainly shows only apatite-type PO_4 bands. Its HPO_4 band at 898 cm^{-1} occurs between band positions of 917 and 861 cm^{-1} for the $HPO_4(5$ and $6)$ groups, respectively. This indicates a shifted HPO_4 position in OCP-CIT as compared to the other OCPCs and is not unexpected because of the different geometry and charge of the citrate ion.

(2) COO and CH_x Bands. Spectra of all six OCPCs have antisymmetric and symmetric COO stretching bands in the 1590–1550-cm^{-1} region and about 1470–1410-cm^{-1} region, respectively, which establish the presence of carboxylate ions in these compounds. All these OCPCs, except OCP-FUM, also have CH_2 bending bands that occur in the same region as their COO symmetric stretching

Table IV. Infrared Wavenumbers (cm^{-1}) and Assignments of Octacalcium Phosphate Carboxylate Bands

OCP-SUCC	OCP-ADIP	OCP-SUB	OCP-SEB	OCP-FUM	OCP-CIT	OCP[a]	assignments
			3570 vvw				OH stretch in HA
	3610 vw	3645 vw				~3600 vvw, sh	ν_3, ν_1 stretch of H-bonded H_2O, HPO_4 (OH stretch)
3525 w	3525 w	3525 w	3525 vw	3525 vw		3525 m	
3410 m, b	3415 m, b	3410 m, b	~3380 w, b	~3380 w, b	~3350 m, b	~3300 m, b	
~3250 m, b	~3225 m, b	~3235 m, b		~3240 m, b		~3090 m, b	
2990 vvw	2983 vvw	2985 vvw	2970 vvw		2965 vvw		CH_2 stretch
	2943 w	2940 w					antisymmetric CH_2 stretch
2925 vvw	2935 w	2935 w	2925 w		2925 vvw		
	2870 vw	2865 vw					symmetric CH_2 stretch
2855 vvw	2855 vvw	2855 vvw	2855 vvw		2850 vvw		
~2460 vw, b	~2460 vw, b	~2460 vw, b	~2400 vw, b	~2400 vw, b	~2300[b] vw, b	2440 vw, b	HPO_4(6) (OH stretch)
1656 w	1661 w	1654 w, b	1652 vw, b	1647 w	1668 vvw, sh	1642 w	ν_2 H_2O bend
	1628 w						
1586 m	1576 m	1575 m	1578 vw, sh	1585 w	1586 m, b		antisymmetric COO stretch
1565 m	1559 m	1560 m	1562 w	1565 m			
			1548[c] w				
1462 w	1467 w	1471 w	1464 vw				CH_2 bend
1453 vw	1457 w	1461 vw		1451[d] w			symmetric COO stretch, CH_2 bend
	1447 w	1441 vw	1442 vw		1449 w, sh		
1435 w	1429 vw	1430 vw, sh		1427[d] w	1415 w		
1406 w	1412 w	1412 w	1410 vw				CH_2 bend
		1358 vvw					CH_2 wag
1330 vw	1331 vw	1337 vw	1348 vvw				
1293 w	1287 w	1291 w	1302 vw	1290 w, b	1300[b] w	1295 w	HPO_4(6)(OH in-plane-bend)
1277 vvw, sh	1278 vvw	1264 vvw	1258 vvw				CH_2 wag, twist
1235 vvw	1239 vvw	1250 vvw					
	1215 vvw	1204 vvw					
				1210 w			CH bend (in-plane)
			1192 vw			1193 w	HPO_4(5)(OH in-plane-bend)
						1137 vvw, sh	ν_3 HPO_4 stretch
1124 s	1124 s	1126 s	1122 s	1118 s		1121 s	ν_3 HPO_4(6) stretch
					1102 s, b		ν_3 HPO_4 stretch
1107 w	1107 w	1107 w	1110 s	1107 s		1103 s	ν_3 HPO_4(5) stretch
1077 s	1076 s	1076 s	1076 s	1078 s		1077 s	ν_3 PO_4, ν_3 HPO_4 stretch
1053 s	1053 s	1054 s	1054 s	1054 s		1055 s	ν_3 PO_4 stretch
1038 s	1038 s	1038 s	1041 s	1038 s	1038 s, b	1037 s	
1026 s	1026 s	1027 s	1027 s	1027 s		1023 s	
~1015 vvw, sh	~1017 vvw, sh	~1017 vvw, sh				~1000 vvw, sh	ν_1 HPO_4 stretch
				976 vvw			CH bend (out-of-plane)
973 vvw, sh	970 vvw, sh	971 vvw, sh					ν_1 PO_4 stretch
962 w	962 w	961 w	963 w	960 w	962 w	962 w	
915 w	913 w	915 w	914 w	919 w		917 w	HPO_4(6)[P-(OH) stretch]
					898 w		HPO_4 [P-(OH) stretch]
			866 vw	864 vw		861 w	HPO_4(5)[P-(OH) stretch]
				814 vw			CH rock ?
805 vvw	735 vvw	785 vvw					CH_2 rock
677 w	671 w	679 w		693 w			COO bend ?
628 vw	628 vw	628 vw	629 vw	628 vw	626 vvw, sh	627 vw	H_2O(4) libration
602 m	601 m	602 m	602 m	601 m	603 m	601 m	ν_4 PO_4 bend
577 w	573 w	575 w	574 w, sh	574 w, sh	580 w, sh	575 w	ν_4 PO_4, ν_4 HPO_4 bend
562 m	561 m	562 m	563 m	563 m	564 m	560 m	ν_4 PO_4 bend
523 vw	519 vw	523 vw	526 vw	526 vw		524 w	ν_4 HPO_4 bend
465 vw	467 vw	467 vw	468 vw	466 vw	468 vw	466 vw	ν_2 PO_4 bend
449 vw	447 vw	449 vw	449 vw	448 vw		449 vw	H_2O libration
343 w	341 w	349 w	346 w	~340 w	~330 w	360 w	Ca-H_2O translation
						~345 w	

[a] Band wavenumbers from part 3,[9] Table I, B form of OCP. [b] These HPO_4 bands in OCP-CIT do not specifically derive from HPO_4(6). [c] This additional band for OCP-SEB may derive from calcium sebacate monohydrate. [d] These OCP-FUM bands derive from COO modes only and not from CH modes. w = weak, m = medium, s = strong, v = very, sh = shoulder, b = broad.

bands; the CH bending bands of OCP-FUM occur at less than 1300 cm^{-1} and not in its COO symmetric stretching region. The antisymmetric COO stretching band for all OCPCs, except OCP-CIT, is split into a doublet; correspondingly, a doublet is also expected for the COO symmetric stretching band. A doublet is observed for the COO symmetric stretch of OCP-FUM (free of interfering CH bands); whereas four to five bands are present in each COO symmetric stretching region of OCP-SUCC, OCP-ADIP, and OCP-SUB that derive from both COO and CH_2 modes. In the spectrum of deuterium substituted OCP-SUCC, discussed later, two of its four bands in this region are attributed to CH_2 bands and the other two to COO symmetric stretching modes. By analogy with OCP-SUCC and OCP-FUM, OCP-ADIP and OCP-SUB are also expected to have at least two COO symmetric stretching bands. The number of observed or inferred COO bands, two each for the antisymmetric and symmetric modes, has bearing on establishing how dicarboxylate ions are incorporated in these compounds.

The OCP-CIT COO bands are broadened, relative to those of the other OCPCs, and show no well-resolved fine structure. These unresolved broad bands indicate a range of COO environments and also indicate a poorly crystallized material as evidenced by its other unresolved IR bands and broadened XRD lines.

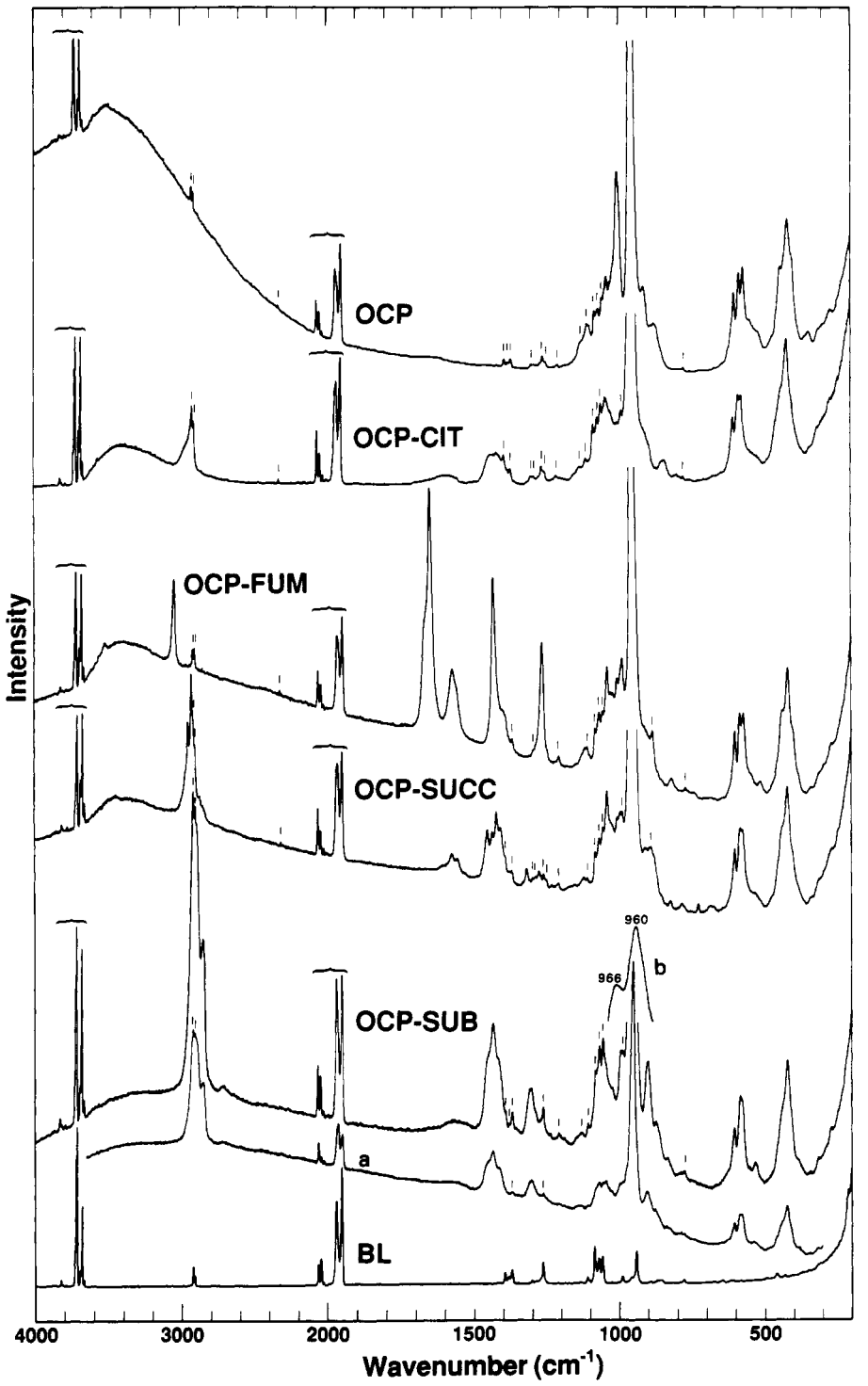

Figure 5. Raman spectra of OCP, OCP-CIT, OCP-FUM, OCP-SUCC, and OCP-SUB from 4000 to 200 cm^{-1} obtained using 488.0-nm wavelength excitation at a power of 175 to 200 mW. OCP-SUB inserts, a and b, are explained in the text. Braces and short vertical lines above each spectrum denote spurious bands arising from its baseline (BL).

The CH_2 stretching bands in the 3000–2850-cm^{-1} region of OCP-CIT and OCP-SUCC are very weak and poorly resolved; OCP-ADIP and OCP-SUB have stronger bands with their antisymmetric and symmetric CH_2 stretching bands both split into doublets. In the CH_2 bending region, about 1480–1410 cm^{-1}, OCP-SUCC, OCP-ADIP, and OCP-SUB all appear to have two or more CH_2 bending bands along with two COO bands. In deuterium-substituted OCP-SUCC (Table VI), the 1462 and 1406 cm^{-1} bands shift to lower wavenumbers and thus arise from CH_2 bending modes. The number of bands observed for the various CH_2 modes also has bearing on how the dicarboxylate ions are incorporated in these compounds; this will be considered in a separate publication.[19]

(3) H_2O Bands. All six OCPCs have a band of medium intensity that extends from about 3700 to 2500 cm^{-1} due to stretching modes of differently hydrogen-bonded H_2O molecules and a weaker band in the 1675–1625-cm^{-1} region due to the H_2O bending modes. The H_2O stretching and

(19) Fowler, B. O.; Marković, M.; Vanderhart, D. L. Manuscript in preparation.

Table V. Raman Wavenumbers (cm^{-1}) and Assignments of Octacalcium Phosphate Carboxylate Bands

OCP-SUCC	OCP-ADIP	OCP-SUB	OCP-SEB	OCP-FUM	OCP-CIT	OCP[a]	assignments
3565 vvw	3568 vvw		3569 w	3570 vvw	3570 vvw		OH stretch in HA
NM[b]	NM[b]	NM[b]	NM[b]	NM[b]	NM[b]	NM[b]	ν_3, ν_1 stretch of H-bonded H_2O
	3522 vw			3530 w			
				3049 m			CH stretch
2982 vw	2980 vw				2979 w		
2963 mw	2938 vw				2930 mw		
2938 w	2913 m	2925 s	2918 m				CH_2 stretch
2881 vw	2896 vw, sh	2905 s	2899 m				
2850 vw	2870 w	2858 m	2883 m				
			2856 m				
	2716 vw	2715 w	2720 w				combination
				1673 m, sh			C=C stretch
				1653 s			
						~1630 vw, b	ν_2 H_2O bend
1580 w	1572 w	~1567 w, b	1566 w, b	1578 mw	~1580 w, b		antisymmetric COO stretch
1561 w	1556 w			1565 mw, sh			
1456 mw	1462 mw, sh	1454 m, sh	1465 mw, sh				CH_2 bend
1440 mw	1449 mw, sh	1439 m	1443 m	1438[c] s	1438 mw		
1425 m	1427 m	1423 m, sh	1419 mw, sh	1406[c] w, sh	1420 mw		symmetric COO stretch, CH_2 bend
1412 mw	1412 m						
				1272 m			CH bend (in-plane)
1322 w	1307 w	1309 mw	1295 mw				
1280 vw	1293 w						
1236 vw	1276 vw						CH_2 wag, twist
1129 vw	1255 vw						
	1241 vw						
	1131 vw						
			1099 vw				C–C stretch
				1119 vw			
						1109 vw	ν_3 HPO_4(5) stretch
						1079 vw	ν_3 HPO_4, ν_3 PO_4 stretch
	1075 w	~1065 mw, b					C′–C″ stretch
1046 w	1048 w	~1050 vw	1046 w	1047 w	1046 w	1050 w	ν_3 PO_4 stretch
	1025 w						C″–C″ stretch
~1004 w	1012 w	1000 w	1006 w	1012 w		1010 m	ν_1 HPO_4 stretch
						1005 w, sh	
				996 w			
~965 s, sh	~965 m, sh	966 s	~965 s, sh	~964 s, sh		966 s	ν_1 PO_4 stretch
958 vs	957 vs	960 vs	959 vs	958 vs	960 vs	957 vs	
~914 w	927 w	907 mw	913 vw	~914 vw		916 w	HPO_4(6)[P–(OH) stretch], C–C′ stretch
~900[d] w, b				~900[d] w, b	~900[d] w, b		HPO_4[P–(OH) stretch] ?
	881 w	879 vw	~880 vw, b			879 w	HPO_4(5)[P–(OH) stretch]
				893 w	848 w		C–C stretch
				828 w			CH bend (out-of-plane)
827 w		835 vw					CH_2 rock
732 w	733 vw						
785 w							
686 w	675 vw						COO bend ?
						618 vw, sh	ν_4PO_4 bend
607 mw	607 mw	608 mw	606 mw	608 mw	607 mw	609 mw	
587 m	590 m	587 m	589 m	591 m	591 m	591 m	ν_4 PO_4, ν_4 HPO_4 bend
580 m	577 m	581 m	579 m	579 m	581 m	578 m	
				~533 vw, b		~556 vw, b	ν_4 HPO_4 bend
~530 w, b	~526 w, b	535 w	~530 vw, b	521 w	~530 w, b	527 w, b	
442 m, sh	443 m	444 m, sh	445 m, sh	445 m	445 m, sh	450 m	ν_2 PO_4 bend
427 m	426 m	426 m	426 m	426 m	425 m	426 m	
408 w, sh	409 w, sh			410 w, sh	408 w, sh	413 m, sh	ν_2 HPO_4 bend
	~389 vw, b	~385 w, b					
						356 w	ν_2 HPO_4(5) bend

[a] Band wavenumbers from part 3,[9] Table I, medium (M) laser power; very weak bands at 1036, ~1025, and 630 cm^{-1} are not included. [b] Spectra of all these compounds have broad unresolved water bands that extend from about 3700 to about 2000 cm^{-1}. [c] These OCP-FUM bands derive from COO modes only and not from CH modes. [d] Band position uncertain because of interfering ghost bands. NM = not measured, w = weak, mw = medium to weak, m = medium, s = strong, v = very, sh = shoulder, b = broad.

bending bands of poorly crystallized OCP-CIT display no fine structure and are not further discussed. All the other OCPCs have a weak band at about 3525 cm^{-1} which corresponds to the 3525-cm^{-1} band of OCP. Since this band persists in these OCPCs, a H_2O position in OCP less prone to change on carboxylate incorporation is expected; a good candidate is H_2O(4) located at the junction of the apatitic and hydrated layers (Figure 6). Consistent with this proposal, all OCPCs except OCP-CIT have corresponding bands each of about the same intensity at about 628 cm^{-1} assigned previously[20] in OCP and here to H_2O(4) libration. Previous assignments[20] for H_2O(4) stretching in OCP were at higher wavenumbers, but 3525 cm^{-1} appears a better choice based on the present data. These data were used in part 3[9] to assign the 3525-cm^{-1} band in OCP to stretching of the H_2O(4) molecules. The OCP-ADIP and OCP-SUB spectra have new distinctive H_2O bands at higher wavenumbers, 3610 and 3645 cm^{-1}, respectively, than those of OCP; these OCPCs contain 6.2 and 8.0 H_2O molecules/formula unit, respectively, from the chemical

Table VI. Infrared and Raman Wavenumbers (cm^{-1}) and Assignments of Octacalcium Phosphate Succinate, OCP-SUCC(H),[a] and Its Deuterated Succinate Analogue, OCP-SUCC(D),[b] in the 1600–1300-cm^{-1} Range

infrared		Raman		
OCP-SUCC(H)	OCP-SUCC(D)	OCP-SUCC(H)	OCP-SUCC(D)	assignment
1586 m	1572 m	1580 w	1569 w	COO antisymmetric stretch
1565 m	1558 m	1561 w	1555 w	
1462 w		1456 mw		CH_2 bend
1453 vw	~1448 w, sh	1440 mw	1437 mw	COO symmetric stretch
1435 w	1431 w	1425[c] m	1410 w	
		1412[c] mw		
1406 w				CH_2 bend
1330 vw		1322 w		CH_2 wag

[a] SUCC(H) = $C_2H_4(COO)_2$. [b] SUCC(D) = $C_2D_4(COO)_2$. [c] Either one of these two bands derive from COO stretching and the other from CH_2 bending.

data. The higher wavenumbers of these bands indicate more weakly bonded H_2O molecules which is in accord with increased volumes of the hydrated layers and probably, in part, due to the hydrophobic nature introduced by the methylene groups. Also, both OCP-ADIP and OCP-SUB spectra have new but less distinctive H_2O bands at about 3415 and 3230 cm^{-1} which probably arise from differently placed but more strongly bonded H_2O molecules. These H_2O stretching changes are also reflected, in part, in the H_2O bending bands for OCP-ADIP and OCP-SUB; this band is broadened to lower wavenumbers corresponding to the more weakly bonded H_2O molecules and to higher wavenumbers corresponding to more strongly bonded H_2O molecules. Spectra of OCP-SUCC and OCP-FUM, containing 6.0 and 5.7 H_2O molecules/formula unit by chemical analyses, respectively, and with less expanded *a* axes are more similar to the OCP spectrum in the H_2O stretching and bending regions and do not display all the additional H_2O spectral features observed for OCP-ADIP and OCP-SUB that contain more H_2O molecules.

Raman Spectra. *(1) PO_4 and HPO_4 Bands.* All OCPCs, except OCP-CIT, have a very strong ν_1 PO_4 band at 958(±2) cm^{-1} and a strong ν_1 PO_4 shoulder at about 965 cm^{-1} which are within a few wavenumbers of those of OCP. The weak ν_3 PO_4 band of OCP at about 1050 cm^{-1} is observed in all OCPCs but very weakly in OCP-SUB. The wavenumbers of the three ν_4 PO_4 bands in the 610–570-cm^{-1} region of the OCPCs agree within a few wavenumbers of those of OCP and their intensities are similar to those of OCP. The ν_2 PO_4 bands of the OCPCs at about 426 cm^{-1} are within ±1 cm^{-1} of that of OCP; the ν_2 PO_4 shoulder near 445 cm^{-1} is present in all OCPC spectra but is less well resolved than the corresponding band in OCP. The overall wavenumber and intensity correspondence between PO_4 bands of the OCPCs and OCP indicate, as did the IR data, the apatite-like structural domains in these OCPCs are very similar to that in OCP.

The medium intensity OCP ν_1 HPO_4 band at 1010 cm^{-1} is markedly reduced in intensity in all OCPCs and the weak intensity OCP ν_3 HPO_4 band at 1109 cm^{-1} is missing or substantially reduced in all OCPCs except OCP-FUM. OCP has a broad ν_4 HPO_4 band in the 570–510-cm^{-1} region with broad maxima at about 556 and 527 cm^{-1}; these band maxima may arise from the different HPO_4(5 and 6) groups. All the OCPCs have weak or broad ν_4 HPO_4 bands near 530 cm^{-1} that are overall weaker in intensity, except for OCP-SUB and OCP-FUM, than the corresponding band in OCP. There appears to be a preferential intensity reduction in the higher wavenumber band at about 556 cm^{-1} in these OCPCs relative to OCP which could result from a preferential reduction in HPO_4(5) groups. The band at about 556 cm^{-1} is, however, too weak and broad to establish this with certainty. The ν_2 HPO_4 bands of OCP occur as a medium intensity shoulder at 413 cm^{-1} and a weak band at 356 cm^{-1}; the 356-cm^{-1} band is essentially missing in all OCPCs and the shoulder near 413 cm^{-1} is reduced in intensity. Because of the marked intensity reduction in the 356-cm^{-1} band, it plausibly arises from the HPO_4(5) group considering the preferential decrease in HPO_4(5) derived from the IR spectra. Changes in the weak bands at 879 and 916 cm^{-1} assigned to HPO_4-[P-(OH)] stretching of HPO_4(5 and 6), respectively, in OCP were difficult to discern and uncertain in the OCPC spectra because of interference from C–C stretching and spurious ("grating ghost") bands in the 900-cm^{-1} region. Consequently, the expected preferential decrease in HPO_4-(5) could not be determined with certainty. Nevertheless, a reduced HPO_4 content is evident in the OCPCs from their overall reduced HPO_4 band intensities. In addition, the HPO_4 bands at 1109 and 356 cm^{-1} which are overall missing in the OCPC spectra are expected to derive from HPO_4(5) groups and are accordingly assigned to this group in Raman spectra of OCP in part 3.[9]

(2) COO and CH_x Bands. OCP-FUM: The CH stretching, CH in-plane bending, and C=C stretching modes[18c] occur as easily detectable medium-to-strong bands at 3049, 1272, and 1653 cm^{-1}, respectively. The weak band at 828 cm^{-1} probably derives from the CH out-of-plane bending or twisting mode. The medium to weak COO antisymmetric band at about 1570 cm^{-1} is composed of a doublet and the strong COO symmetric stretching band at 1438 cm^{-1} has a weak shoulder at 1406 cm^{-1} which is probably a second COO symmetric stretching component.

OCP-CIT, OCP-SUCC, OCP-ADIP, OCP-SUB, and OCP-SEB: All these OCPCs have increasing intensity CH_2 stretching bands in the above sequence concomitant with their increasing CH_2 contents, except impure OCP-SEB, which has about one-third the theoretical sebacate content. The positions of the two strongest CH_2 stretching bands of OCP-CIT and OCP-SUCC, both containing only α-CH_2 groups, occur at higher wavenumbers than those of the other three OCPCs.

The COO antisymmetric stretching bands at about 1570 cm^{-1} of OCP-SUCC and OCP-ADIP both occur as weak doublets and OCP-SUB, OCP-SEB, and OCP-CIT have broad unresolved weak bands in this region. In the COO symmetric stretching and CH_2 bending region, about 1470–1410 cm^{-1}, OCP-CIT has one broad band composed of a doublet; OCP-SUB and OCP-SEB each have three bands; and OCP-SUCC and OCP-ADIP each have four bands. In the spectrum of deuterium-substituted OCP-SUCC (Table VI), two of these four bands have shifted to lower wavenumbers and thus arise from CH_2 bending modes.

The remaining unshifted two bands arise from COO symmetric stretching modes and their number, two, is in accord with the presence of two COO antisymmetric stretching bands. By analogy with deuterium-substituted OCP-SUCC, two of these four bands of OCP-ADIP are expected to arise from CH_2 bending modes and the other two from COO symmetric stretching modes. In the corresponding regions of OCP-SUB and OCP-SEB, only three bands are resolved in each spectrum, and it is uncertain whether more than one COO symmetric stretching band is present.

(3) *H_2O Bands.* All these OCPCs, including OCP, have broad overall unresolved bands extending from about 3700 to 2000 cm^{-1} that derive from stretching modes of their hydrogen-bonded water molecules. Only OCP-ADIP and OCP-FUM showed additional weak bands near 3525 cm^{-1} on these broad bands. Consequently, no meaningful structural information on their water components was obtainable from the spectra. All these OCPCs, except OCP-SUB, have very weak bands at about 3570 cm^{-1}, not evident in Figure 5 but on expanded scale, that are attributable to OH stretching from HA. The HA content was estimated to be a few mass percent and highest for OCP-SEB.

Combined Infrared and Raman Data. The number and coincidence of the IR and Raman bands of the COO and CH_2 modes of the dicarboxylate ions have bearing on their geometry and how they are incorporated in the OCPCs; however, interpretation of the spectral data is not straightforward. The splitting of the antisymmetric and symmetric COO stretching modes each into two bands in both the IR and Raman may arise from several sources: distortion of the ions to lower symmetries, two nonequivalent ions, and factor group coupling between two identical ions.

There are two dicarboxylate ions per OCPC unit cell and thus four COO groups. Depending on the point-group symmetry of each dicarboxylate ion, these four COO groups can be all equivalent, all nonequivalent, or combinations of equivalent and nonequivalent groups. The possible point group symmetries for the individual dicarboxylate ions studied here are C_{2h}, C_i, C_s, C_2, and C_1. For C_{2h} and C_i symmetries (two equivalent COO groups), the antisymmetric and symmetric COO stretching modes of a dicarboxylate ion are each predicted to have one IR band and one noncoincident Raman band, whereas for the lower symmetries C_s, C_2, and C_1 (all having two nonequivalent COO groups) two IR and two coincident Raman bands are predicted for each of these modes. The OCP-SUCC, -ADIP, and -SUB compounds have interfering CH_2 bending bands in the COO symmetric stretching region; these were identified using deuteration for OCP-SUCC only (Table VI), and OCP-FUM does not have interfering bands in this region. Thus, COO bands of only OCP-SUCC and OCP-FUM will be discussed in the present paper. In addition, to complement the IR and Raman data, ^{13}C NMR spectra of OCP-SUCC and OCP-FUM were obtained.

OCP-SUCC (Table VI) and OCP-FUM (Tables IV and V) each have two antisymmetric and two symmetric COO stretching bands in both IR and Raman; the OCP-SUCC IR and Raman bands are noncoincident (differences in band positions of ≥ 3 cm^{-1} were considered noncoincident), and three of the four bands of OCP-FUM are noncoincident. Six cases of symmetric and/or nonsymmetric dicarboxylate ions occupying two equivalent sites or two nonequivalent sites in the OCPC structure were considered. The observed IR and Raman data for the two COO stretching bands agree with two of these six cases: (A) two identical symmetric anions (C_{2h} or C_i symmetry) on two equivalent sites yielding two predicted noncoincident bands in both the IR and Raman along with additional splitting of each band into two components due to factor group coupling between modes of the identical anions yielding a final four noncoincident bands in both the IR and Raman, and (B) two different symmetric (C_{2h} or C_i symmetry) ions on two nonequivalent sites also yielding, the same predicted final spectra as case (A), four noncoincident bands in both the IR and Raman spectra.

NMR spectra of OCP-SUCC and OCP-FUM show two nonequivalent COO groups are present in each compound. This NMR COO group nonequivalence indicates the two dicarboxylate ions per unit cell are either (1) nonsymmetric (C_s, C_2, or C_1 symmetry) with both ions having the same symmetry on two equivalent sites or (2) symmetric (C_{2h} or C_i symmetry), but each ion has different symmetric symmetry on two nonequivalent sites. The NMR data rule out IR and Raman case (A) which would have four equivalent COO groups; therefore, factor group coupling does not cause splitting of the IR and Raman COO stretching bands. The IR and Raman data are inconsistent with NMR case (1) because coincident IR and Raman bands are predicted but are consistent with NMR case (2) where noncoincident IR and Raman bands are predicted and overall observed. Consequently, the combined IR–Raman–NMR data best agree with two different symmetric ions on two nonequivalent sites. However, this interpretation is equivocal. The NMR data clearly show two nonequivalent COO groups. The numbers of IR and Raman bands also indicate two nonequivalent COO groups (provided that no factor group band splittings occur). The overall noncoincidence of IR and Raman bands was the deciding factor to indicate two symmetric anions on two nonequivalent sites. The same number of IR and Raman bands, four but all coincident, would indicate two identical nonsymmetric ions on two equivalent sites or NMR case (1).

A more detailed combined IR–Raman–NMR study of carboxylate ion incorporation, utilizing both COO and CH_2 groups, in OCP-SUCC, -ADIP, -SUB, -FUM, and -CIT will be given in a separate paper.[19]

Structural Considerations. The OCPCs derive from and are structurally similar to their parent compound OCP. The structure of OCP, shown in Figure 6, can be considered to consist of two layers parallel to (100), a layer which is related to that of HA (apatitic layer, denoted by dotted circles) and a layer which contains all the water molecules (hydrated layer, denoted by unfilled circles). The crystallographic center of symmetry is at ($^1/_2$, $^1/_2$, $^1/_2$), between O5 water molecules. The phosphate groups $PO_4(1)$ and $PO_4(4)$ lie within the apatitic layer. The phosphates $PO_4(2)$ and $PO_4(3)$ and hydrogen phosphate $HPO_4(6)$ lie at the junction of the apatitic and hydrated layers. The hydrogen phosphate $HPO_4(5)$ bridges calcium atoms within the hydrated layer. The two pairs of $HPO_4(5)$ groups have inversion centers at ($^1/_2$,0,0) and ($^1/_2$,1,0). The $HPO_4(5)$ and $HPO_4(6)$ groups are crystallographically nonequivalent.

The combined chemical, XRD, and particularly spectroscopic data were utilized to elucidate and to infer structural details of the OCPCs. From the chemical

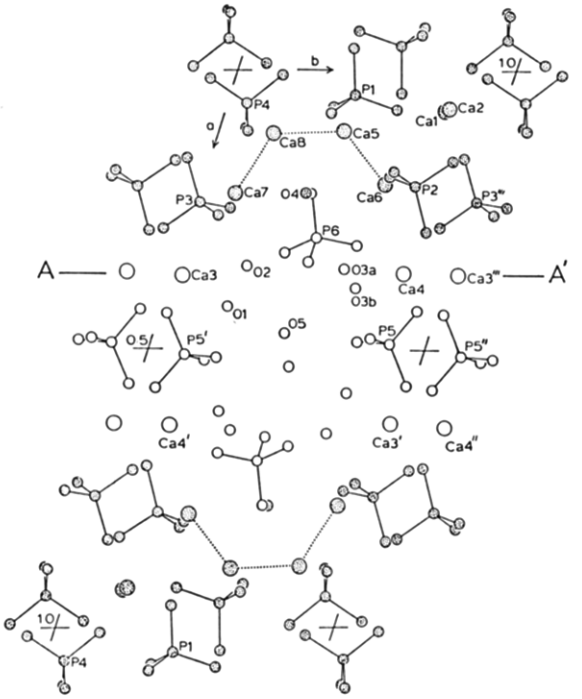

Figure 6. Structure of OCP projected down the *c* axis. The unfilled circles (O1, O2, O3a, O3b, O5) and dotted circle O4 are water molecules; hydrogen atoms are not shown. After ref 21.

composition and IR and Raman spectra, it was determined that there were no significant changes in the number and in the positions of PO_4 groups compared to those of OCP. The substantial reduction of $HPO_4(5)$ IR bands, persistence of $HPO_4(6)$ IR bands, and concomitant *a*-axis unit-cell expansion from XRD data established that $HPO_4(5)$ ions present in OCP were replaced by dicarboxylate ions in the OCPCs.

The most probable positions for incorporation of dicarboxylate ions in the hydrated layer were previously predicted in two structural models (I[3] and II[21]). Figure 7 schematically shows models I and II for dicarboxylate incorporation. In model I[3] it was predicted that the two Ca(4)–$HPO_4(5)$–Ca(3′) and Ca(3″)–$HPO_4(5'')$–Ca(4″) pillars in OCP (Figure 6) are substituted by two Ca–dicarboxylate–Ca pillars (Figure 7, model I, positions 1 and 1′) in the OCPCs. In model II[21] which was developed for OCP-SUCC and based on structural similarity of OCP and calcium succinate trihydrate, it was predicted that two structurally nonequivalent dicarboxylates are present in the structure; the first one is incorporated in the space of the two HPO_4 groups (5 and 5″) in OCP (Figure 6; Figure 7, model II, position 2) and the second dicarboxylate bridges Ca(3) and Ca(3′) (Figure 6) diagonally throughout the space occupied by water molecules (Figure 7, model II, position 3). The combined IR–Raman–NMR data for COO groups of OCP-SUCC and OCP-FUM indicate that the two dicarboxylate ions per OCPC unit cell are on two nonequivalent sites; this supports model II.

In addition, concomitant with dicarboxylate ion incorporation and *a*-axis expansion, a large increase in volume

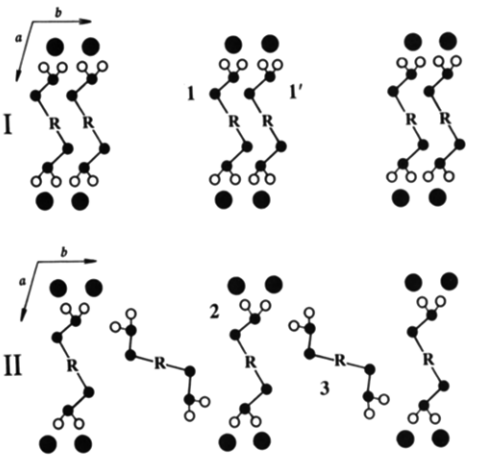

Figure 7. Schematic models (I and II) for positions of dicarboxylate ion incorporation in OCPCs projected down the *c* axis. Large filled circles denote calcium, small filled circles denote carbon, unfilled circles denote oxygen, and R denotes $(-CH_2-)_n$. The positions of calcium atoms are related to those denoted by Ca3 and Ca4 in the hydrated layer of OCP (Figure 6).

of the hydrated layers occurs in the OCPCs. These volumes in OCP-SUCC, OCP-ADIP, and OCP-SUB are about 1.5, 2.0, and 2.5 times, respectively, that of OCP but contain 1.20, 1.24, and 1.60 times respectively, the H_2O content of OCP. These disproportionately low amounts of H_2O in the OCPCs result in considerable empty space in their hydration layers as compared to that in OCP. A diagonally incorporated dicarboxylate ion (Figure 7, model II, position 3) would partially fill this empty space; filling this void could be a contributing factor favoring model II type incorporation.

It is of interest why the $HPO_4(5)$ ions, rather than the $HPO_4(6)$ ions, are preferentially replaced by the dicarboxylate ions. A plausible reason is that in model I (Figure 7) the two dicarboxylate ions 1 and 1′ can have an inversion center between them and in model II (Figure 7) dicarboxylate ions 2 and 3 can each be located on centers of symmetry. This symmetric type of incorporation is expected to favor lattice repeat. On the other hand, the $HPO_4(6)$ ion does not reside on a center of symmetry. Although a dicarboxylate ion replacement for $HPO_4(6)$ could occur, the observed data showing it does not indicate that this site is not favorable for Ca–dicarboxylate bonding and/or lattice repeat. Moreover, because $HPO_4(6)$ lies on the boundary between hydrated and apatitic layers its replacement by long-chain dicarboxylates should cause considerable changes in the whole structure including the apatitic layer.

Acknowledgment. We thank M. Mathew, ADAHF, PRC, NIST for advice and helpful discussions on the structure of OCP and W. E. Roberts, Building and Fire Research Laboratory, NIST, for TG analyses. This work was supported by the USA–Yugoslav Joint Fund for Scientific and Technological Cooperation in collaboration with the National Institute of Standards and Technology, Gaithersburg, MD (Grant PN 776), by the Ministry of Science, Technology and Informatics of Croatia and, in part by USPHS Research Grant DE-05030 to the American Dental Association Health Foundation by the National Institutes of Health and is part of the dental research program conducted by NIST in cooperation with ADAHF. M.M gratefully acknowledges financial support from the Fulbright Scholarship Exchange Program.

(20) Berry, E. E.; Baddiel, C. B. *Spectrochim. Acta* **1967**, *23A*, 1781.
(21) Mathew, M.; Brown, W. E. *Bull. Chem. Soc. Jpn.* **1987**, *60*, 1141.
(22) Certain commercial materials and equipment are identified in this paper to specify the experimental procedure. In no instance does such identification imply recommendation or endorsement by the National Institute of Standards and Technology, the National Institutes of Health, or the ADA Health Foundation or that the material or equipment identified is necessarily the best available for the purpose.